Journal of Earthquake Engineering

ISSN: 1363-2469 (Print) 1559-808X (Online) Journal homepage: www.tandfonline.com/journals/ueqe20

Seismic Response of Rocking Precast Concrete Cladding System in a Full-Scale Three-Storey Building

R. K. Shrestha , J. Bhatta , R. P. Dhakal, T. J. Sullivan , A. Tiwari , Z. Yan , G. A. MacRae , Y. Zhang , Z. Li , P. Xiang , L. J. Jia , S. Ramhormozian , G. C. Clifton , P. Quenneville , G. Rodgers & X. Zhao

To cite this article: R. K. Shrestha , J. Bhatta , R. P. Dhakal, T. J. Sullivan , A. Tiwari , Z. Yan , G. A. MacRae , Y. Zhang , Z. Li , P. Xiang , L. J. Jia , S. Ramhormozian , G. C. Clifton , P. Quenneville , G. Rodgers & X. Zhao (28 May 2026): Seismic Response of Rocking Precast Concrete Cladding System in a Full-Scale Three-Storey Building, Journal of Earthquake Engineering, DOI: 10.1080/13632469.2026.2677799

To link to this article: https://doi.org/10.1080/13632469.2026.2677799

Published online: 28 May 2026.

JOURNAL OF EARTHQUAKE ENGINEERING
https://doi.org/10.1080/13632469.2026.2677799

Seismic Response of Rocking Precast Concrete Cladding System in a Full-Scale Three-Storey Building

R. K. Shrestha[a], J. Bhatta[a], R. P. Dhakal[a], T. J. Sullivan[a], A. Tiwari[a], Z. Yan[b], G. A. MacRae[a], Y. Zhang[a], Z. Li[c], P. Xiang[c], L. J. Jia[c], S. Ramhormozian[b], G. C. Clifton[d], P. Quenneville[d], G. Rodgers[e], and X. Zhao[c]

[a]Civil and Environmental Engineering, University of Canterbury, Christchurch, New Zealand; [b]Built Environment Engineering, Auckland University of Technology, Auckland, New Zealand; [c]College of Civil Engineering, Tongji University, Shanghai, China; [d]Civil and Environmental Engineering, University of Auckland, Auckland, New Zealand; [e]Mechanical Engineering, University of Canterbury, Christchurch, New Zealand

ABSTRACT

Precast concrete cladding systems are not only vulnerable to seismic damage but also pose a life-safety hazard due to the potential for panel detachment and falling during earthquakes. However, research assessing seismic response of the cladding systems installed on full-scale buildings under dynamic loading is limited. To address this gap, an experimental programme was undertaken as part of the RObust BUilding SysTem (ROBUST) project. In this study, rocking cladding panels were installed on the upper two storeys of a full-scale, three-storey steel frame building specimen. The building was subjected to unidirectional and bidirectional horizontal ground motions, inducing peak inter-storey drift ratios of up to 1.71% and peak floor accelerations of up to 0.95 g at the storeys where the cladding panels were installed. This paper presents the experimental findings on the seismic response of the rocking cladding system, including peak rocking displacements and component acceleration amplification factors. Physical damage observations are categorised by severity and correlated with inter-storey drift ratios. Damage to the sealant was first observed at a peak inter-storey drift ratio of 0.51% in one of the cladding systems, while the remaining eleven cladding systems sustained drift levels up to 1% without any damage. Additionally, vibration modes and corresponding frequencies are identified. The results demonstrate that the rocking cladding system effectively accommodated the imposed seismic demands without severe damage or collapse, highlighting the rocking mechanism as a low-damage solution for precast concrete cladding systems.

ARTICLE HISTORY
Received 23 November 2025
Accepted 6 May 2026

KEYWORDS
Low-damage connection; rocking cladding system; shake table test; component acceleration amplification factor; damage states

1. Introduction

Damage to non-structural elements (NSEs) during past earthquakes has led to substantial economic losses, functional disruptions, injuries, and fatalities (Dhakal et al. 2016; Filiatrault and Sullivan 2014; Miranda et al. 2012; Villaverde 1997). In many cases, the severity of NSE damage has exceeded structural damage (Baird and Ferner 2017; Dhakal 2010; FEMA 2011; Sagbas et al. 2024). Consequently, damage to NSEs dominates building losses (repair and downtime) in minor to moderate earthquakes (Dhakal 2024). Moreover, their construction cost (Khakurel et al. 2020; Taghavi and Miranda 2003) as well as seismic loss contributions (Bradley et al. 2009; Dhakal, Mander, and Xu 2010; O'Reilly et al. 2018) can surpass those of structural components. Among

CONTACT R. K. Shrestha rajesh.shrestha@pg.canterbury.ac.nz Civil and Environmental Engineering, University of Canterbury, Private Bag 4800, Christchurch 8140, New Zealand

various types of NSEs, building façade systems can account for up to 18% of a building's initial cost, making them one of the most expensive NSEs (Lam and Gad 2002; Taghavi and Miranda 2003).

Precast concrete cladding has been extensively used worldwide, including in New Zealand, as an exterior façade that encloses buildings and protects interior spaces from environmental exposure. However, repeated instances of seismic damage to cladding systems have been reported in past earthquakes such as the 2009 L'Aquila earthquake (Toniolo and Colombo 2012), the 2010 Chile earthquake (Miranda et al. 2012), the 2010 Darfield earthquake (Dhakal 2010), the 2011 Christchurch earthquake (Baird et al. 2014), the 2012 Emilia earthquake (Bournas, Negro, and Taucer 2014), and the 2016 Kaikōura earthquake (Baird and Ferner 2017). During these earthquakes, typical damage included hairline cracks and corner crushing of cladding panels, sealant tears, connection failures, and bolt locking within slotted holes. Beyond these forms of damage, panel detachment and falling during seismic events pose life-safety hazards (Baird, Palermo, and Pampanin 2011; Villaverde 1997).

1.1. Past Studies on Cladding Panel Connections and Their Seismic Performance

Cladding panels are typically connected to the primary structure using two types of connections: tie-back (or push-pull) and bearing connections. Because these panels are sensitive to both storey drift and floor acceleration, their connection systems must be designed to accommodate both types of seismic demand. Steel tie-back connections are commonly adopted to resist out-of-plane loads while allowing in-plane movement via translation or rocking mechanisms. Translational behaviour is typically facilitated by combining horizontally slotted tie-backs and fixed bearing connections, while rocking motion is enabled by vertically slotted tie-backs combined with bearing connections. Tie-backs may be provided at the top and bearings at the bottom, alternatively, bearings at the top and tie-backs at the bottom (Hutchinson et al. 2014; M. L. Wang 1987). According to the Precast/Prestressed Concrete Institute (PCI 2007), tie-back connections can accommodate displacement demands through sliding (e.g. slotted or oversized holes), flexing (e.g. bending steel rods), or alternative mechanisms that provide equivalent displacement capacity or ductility.

Extensive experimental studies have investigated the seismic performance of cladding panels with various connection details. Early research included a full-scale pseudo-static test on a six-storey steel building equipped with cladding panels using typical US and Japanese connections (M. L. Wang 1987). Rihal (1988) conducted a series of component- and system-level tests, including static component tests of cladding panel connections, cyclic in-plane racking tests on full-size panels, and dynamic tests on a reduced-scale two-storey steel building with cladding panels. In the last decade, several studies have focused on innovative connection systems. Baird (2014) performed experimental tests with various traditional connections (tie-back rod and slotted plate) and identified their poor performance through numerical analysis on a case study building. To address this, a low-damage connection consisting of U-shaped flexural plate dissipators was proposed to accommodate large displacements while minimising force transfer into the cladding panels. Bhatta et al. (2020) introduced a vertical sliding connection that enabled the cladding panels to exhibit a rocking mechanism and sustain no significant damage up to 4% drift under quasi-static cyclic loading, with only sealant tearing observed at 1.92% drift. A study by Bianchi et al. (2021) involved three-dimensional shake table tests on innovative glass fibre reinforced concrete cladding panels integrated into a half-scale low-damage timber-concrete structural system. Furthermore, Bhatta, Dhakal, and Sullivan (2023a) tested two subassemblies of four rocking cladding panels under quasi-static reverse cyclic tests, showing no noticeable damage up to 2% drift, though adhesion failure of the sealant joint occurred at 1.4% drift.

Despite these advances, few studies have investigated the seismic performance of cladding systems under dynamic loading on full-scale buildings. McMullin et al. (2012) conducted shake table tests using three-dimensional ground motions on corner panel assemblies mounted on a five-storey steel moment frame building. The rocking cladding system performed well, with no observed damage up to peak floor accelerations of 0.8 g and inter-storey drifts of 0.17%. Similarly, Pantoli et al. (2013) performed

unidirectional dynamic tests on cladding panels with push-pull connections (sliding and flexing rod connections) installed on the upper two levels of a full-scale five-storey reinforced concrete building.

1.2. Past Studies on Component Acceleration Amplification of Cladding Systems

Despite growing research on drift-compatible and low-damage connections for cladding systems, limited work has focused on quantifying seismic forces generated by acceleration demands in these systems. The component acceleration amplification factor, defined as the ratio of peak component acceleration to peak floor acceleration, is a critical parameter for estimating seismic forces in cladding systems. Kamau-Devers (2016) conducted a study to determine the in-plane and out-of-plane amplification factors for rocking cladding systems common in the US. Pantoli and Hutchinson (2019) also evaluated these factors for service level and design level ground motions, which were significantly larger than those prescribed in ASCE 7–10 (2010). Additionally, Huang, Lu, and Mosalam (2018) reported maximum in-plane and out-of-plane amplification values of 3.67 and 2.86, respectively, for granite cladding panels.

1.3. Past Studies on Natural Frequency of Cladding Systems

Natural frequency (or fundamental period) of NSE is one of the key characteristics that influences its seismic demand. It is known that acceleration amplification depends on the proximity of the component period to the structural period, as well as on the damping of both the structure and the component (Haymes, Sullivan, and Hare 2025; Rashid, Dhakal, and Sullivan 2021; X. Wang and Hutchinson 2024; Welch and Sullivan 2017). Moreover, natural frequency is used for the classification of components. ASCE/SEI 7-22 (2022) classifies a component as rigid if its fundamental period is less than or equal to 0.06 s (i.e. natural frequency $\geq$ 16.7 Hz) and flexible if its fundamental period is greater than 0.06 s (i.e. natural frequency $<$ 16.7 Hz). Despite its importance, quantification of the natural frequency of the cladding system has received limited attention. Merrick et al. (2003) and Pantoli and Hutchinson (2015) are among the few studies that have evaluated these frequencies. Pantoli and Hutchinson (2015) identified the out-of-plane frequency as low as 7.90 Hz, and the vertical mode frequency as low as 13.9 Hz, suggesting that cladding panels may not always behave as rigid components.

1.4. Research Objectives

To address these gaps (limited research on full-scale dynamic testing, as well as on acceleration amplification factor and natural frequency of cladding system), an experimental study was undertaken as part of the RObust BUilding SysTem (ROBUST) project at the International Joint Research Laboratory of Earthquake Engineering (ILEE), Tongji University, Shanghai, China. The study involved full-scale shake table tests on a three-storey steel frame building subjected to both unidirectional and bidirectional horizontal shaking (Dhakal et al. 2020; MacRae et al. 2020). Vertical ground motion was not considered in the experimental programme because the shake table could provide seismic excitation only in two horizontal directions. Cladding panels with vertical sliding connections were installed on the upper two storeys of the building. The objectives of this investigation of the seismic response of rocking cladding systems are to:

(1) evaluate the performance of different cladding systems with respect to their connection configurations,
(2) document damage observations and correlate them with inter-storey drift ratios of the structure,
(3) compare experimentally measured peak rocking displacements with theoretical predictions,
(4) quantify component acceleration amplification factors, and
(5) identify vibration frequencies to assess the dynamic characteristics of the cladding system.

2. Experimental Programme

2.1. Primary Structure

The ROBUST tested building consisted of two bays in the longitudinal (North-South/X) direction and one bay in the transverse (East-West/Y) direction, with plan dimensions of 7.25 m × 4.75 m and an inter-storey height of 3.0 m. The composite flooring system, ComFlor® 80 (Steel & Tube Ltd 2016), featuring a trapezoidal steel deck with a concrete topping, was used. The structure was designed as an office building with Importance Level 2 (NZS 1170.0 2002), located on shallow soil classified as Subsoil Class C in Wellington (NZS 1170.5 2016).

The structural configuration during cladding system testing consisted of a lateral load-resisting system formed by a Moment Resisting Steel Frame (MRSF) incorporating Optimized Sliding Hinge Joints (OSHJs) at the beam-to-column connections, referred to as MRSF-OSHJ, as shown in Fig. 1a. The OSHJs were applied only in the right-hand side bay, while the left-hand side bay was pinned. In the transverse (EW/Y) direction, the lateral load-resisting system comprised a V-braced Concentrically Braced Frame (CBF) with Symmetric Friction Connections (SFC) incorporating partially deflected Belleville Springs (SFCBeSs) at the brace-to-gusset plate connections, denoted as CBF-V-SFCBeSs, as depicted in Fig. 1b. Further details of the primary structural system can be found in Yan et al. (2023) and MacRae et al. (2024).

2.2. Cladding System

2.2.1. Geometry and Nomenclature

Twelve full-storey cladding panels of varying widths, incorporating vertical sliding connections developed by Bhatta et al. (2020), were installed on the second and third storeys of the test structure, with six panels per storey (Fig. 2). Their detailed dimensions are given in Table 1. The panels were arranged into three subassemblies: (1) panels with equal aspect ratios, (2) panels with unequal aspect ratios, and (3) corner panels consisting of flat and L-shaped configurations, positioned on diagonally

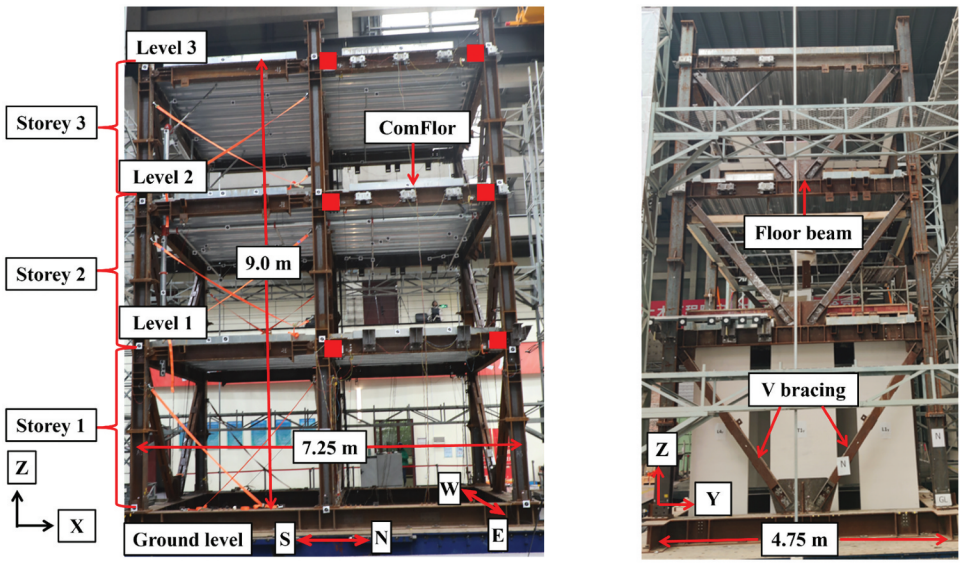

Figure 1. Photographs of the full-scale three-storey steel test structure: (a) longitudinal (NS/X) direction (MRSF–OSHJ system – OSHJ locations highlighted in red); (b) transverse (EW/Y) direction (CBF–V–SFCBeSs system).

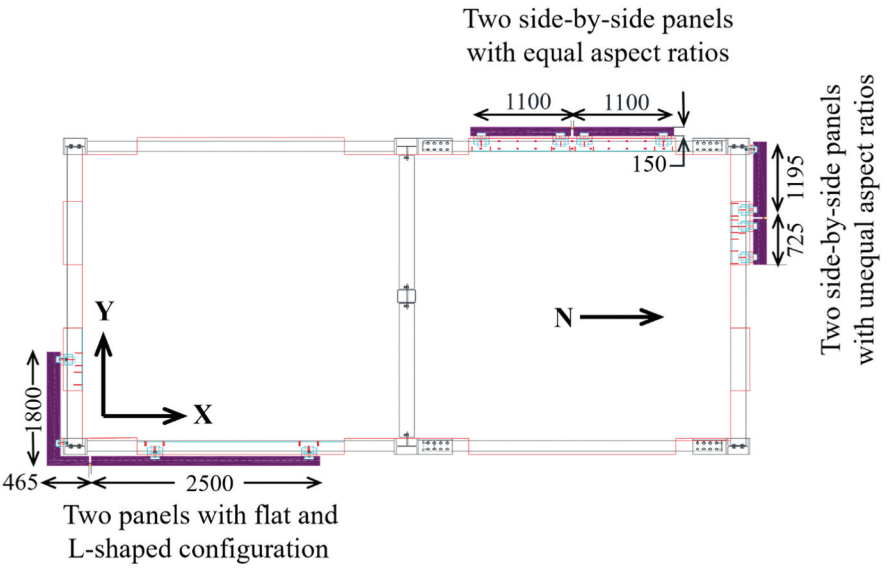

(a)

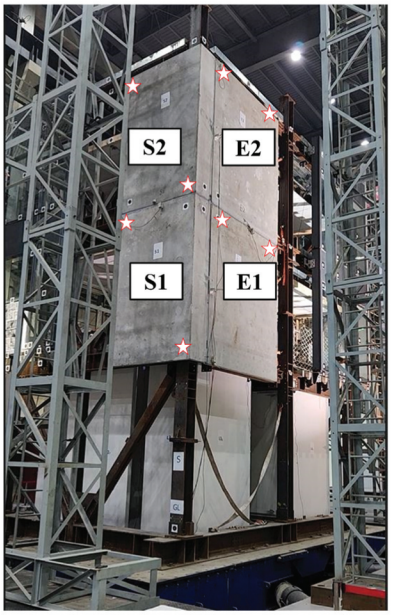

(b)

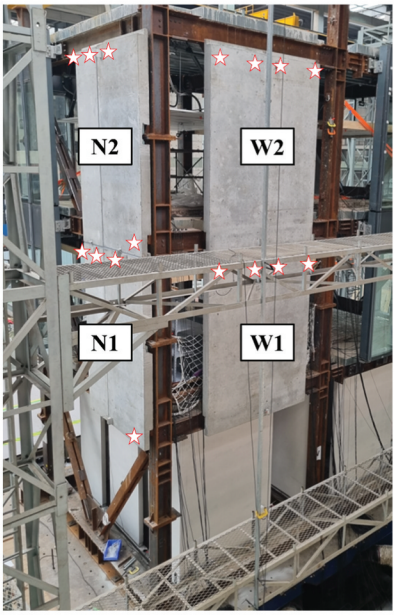

(c)

Figure 2. (a) Layout of cladding panels on the floors (plan view); (b) elevation view of the corner configuration with L-shaped and flat panels; (c) elevation view of panels with equal (right) and unequal aspect ratios (left). White stars represent tack-welds between the nuts, and the horizontally slotted angles to prevent horizontal movement of the cladding panels relative to the structure.

Table 1. Dimensions of different cladding panel configurations installed in the test structure.

Cladding panel configuration	Height (mm)	Width (mm)	Thickness (mm)
L-shaped (south elevation – S1, S2)	3050	Main leg = 1800 Return leg = 465	150
Flat panel (east elevation – E1, E2)	3050	2500	150
Equal aspect ratio (west elevation –W1, W2)	3050	1100	150
Unequal aspect ratio (north elevation – N1, N2)	3050	B_1 = 1195 B_2 = 725	150

opposite corners of the building, as depicted in Fig. 2a. These panels added a substantial weight of approximately 200 kN to the structure, while the weight of the tested structure alone was about 820 kN. The panels on the east and south elevations weighed 57 kN and 48 kN, respectively, while those on the west and north elevations weighed 52 kN and 43 kN. Cladding panels were labelled with capital letters indicating their building elevation, i.e. north (N), south (S), east (E), and west (W), followed by a numerical subscript, as shown in Fig. 2b,c.

2.2.2. Specimen Design and Details

Each panel consisted of four steel-embeds with vertical slots (vertical sliding connections) on their inner faces and two weld-plates to rest on rectangular hollow sections (RHS) at the base, which served as bearing connections, as shown in Fig. 3. Details of the steel-embed and weld-plate are illustrated in Figs. 4 and 5, respectively. The steel-embeds allow the cladding panels to accommodate inter-storey drift through a rocking mechanism that causes bolt sliding within the vertical slots, while resisting out-of-plane forces. Bhatta et al. (2020) compared the seismic performance of this rocking cladding system with that of conventional horizontal sliding connections (horizontal-slots and threaded rods) documented in the literature. Their study found the rocking cladding system to be seismically more resilient than the traditional alternatives. Furthermore, this system offers additional advantages: it prevents the formation of large vertical joint gaps between panels at building corners, and its installation and adjustment process is relatively simple and efficient. This efficiency can potentially

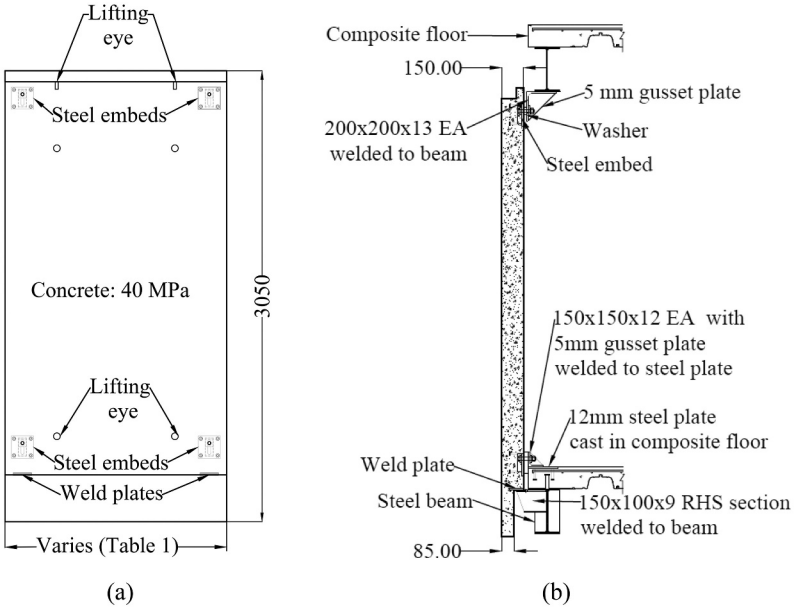

Figure 3. Panel details (dimensions in mm): (a) front view; (b) sectional side view.

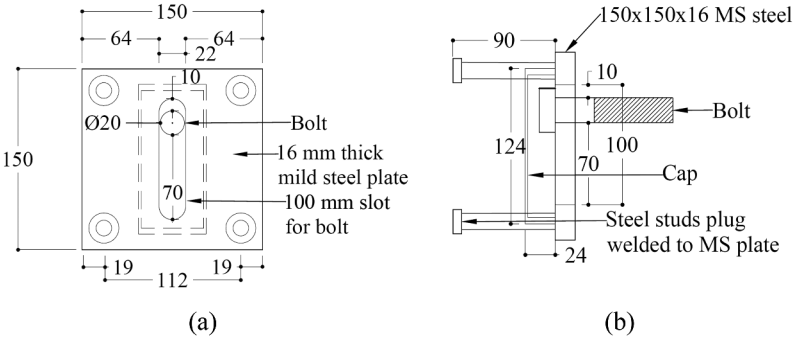

Figure 4. Steel-embed details (dimensions in mm): (a) front view; (b) side view.

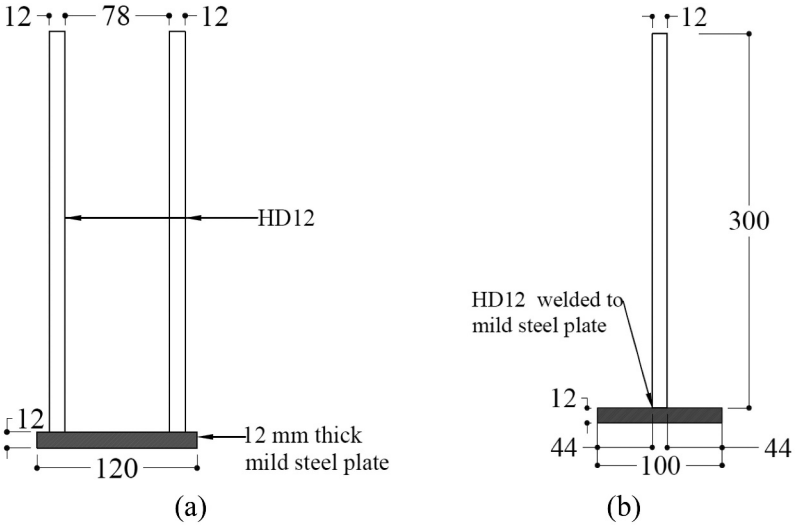

Figure 5. Weld-plate details (dimensions in mm): (a) front view; (b) side view.

reduce on-site labour, crane time, and associated costs (Bhatta et al. 2020; Bhatta, Dhakal, and Sullivan 2023b). Additionally, the weld-plates transfer the gravity loads of the panels to the main structure and act as points of rotation for the panels and prevent local concrete crushing or chipping during rocking. Bottom bearing connections offer several practical and structural advantages: they facilitate easier erection, place the concrete panel in compression (the preferred stress state) rather than tension, and provide redundancy, such that if the bottom bearing support fails, the upper tie-back connections can support the panel's dead load (M. L. Wang 1987). In addition to the steel-embed connections, each panel included four anchors (lifting eye) for face-lifting during transportation and two for top-lifting during installation and demoulding (Fig. 3a). The cladding panels were connected to the structure using four steel angles with horizontal slots. Two of the steel angles were welded to the bottom flanges of the top beams, while the other two were welded to the steel plate embedded in the composite floor slab, as shown in Fig. 3b.

Referring to the distance between bearing connections as "r", which can also be taken approximately equal to the width of the panel, the length of the vertical slot "y" in the steel-embeds required to accommodate inter-storey design drift "θ" is given by Eq. (1) (Bhatta et al. 2020):

$$y = \theta \times r \tag{1}$$

In this test, the length of the vertical slot was 100 mm, and the diameter of the bolt was 20 mm. Assuming 10 mm additional length of the slot required for out-of-plane deformation and tolerance for construction and installation errors, the effective vertical slot provided in the steel-embed is given by: total slot length – diameter of bolt – tolerance = 100 – 20–10 = 70 mm. Therefore, the drift capacity of the largest panel (with width = 2500 mm, taken as equal to r) is conservatively estimated as 2.80% $\left(=\frac{70}{2500}\ \text{x}\ 100\right)$.

Under small seismic excitation, the clearance between the bolt and the vertical slot (22 mm – 20 mm = 2 mm, as shown in Fig. 4) closes before rocking initiates, producing a small initial movement that slightly delays the onset of rocking response by approximately 0.08% drift. Once the bolt contacts the edge of the vertical slot, the connection engages fully, and the panel exhibits its rocking behaviour as intended. As a result, the slot clearance may delay the early response at low excitation levels but does not significantly affect the rocking rotation or vertical sliding during large shaking. Such small clearances are necessary for fabrication and are unlikely to cause detrimental effects in practical applications when properly installed. It is recommended to avoid the bolt threads within the vertical slot plate thickness during construction and installation of the panels, as the threads may lock the panel and potentially provide an undesirable gravity restraint and act as pivot point of rotation as observed in Bhatta, Dhakal, and Sullivan (2023b).

When two adjacent full storey-height panels simultaneously rock under relative lateral floor displacements, shear deformation and shear forces are imposed on the sealant at the interface of the two panels. Thus, for a sealant with ultimate shear strain capacity γ_{ult} and full storey-height panels of width "b," the minimum vertical joint width required to avoid tearing of the sealant at a storey drift of "θ" is (Bhatta et al. 2020):

$$w_{min} = \frac{b\theta_s}{\gamma_{ult}} \tag{2}$$

The average width of the vertical joint provided in the test setup was 25 mm. Using a sealant with γ_{ult} = 125% (Dal Lago et al. 2017), the inter-storey drift ratio at which the tearing of the sealant is expected to occur at the vertical joint between the east and south elevation panels, considering the largest panel of 2500 mm width, can be estimated as $\theta_s = \frac{25\ \text{x}\ 125}{2500} = 1.25\%$. For aesthetic consistency, the horizontal joint width was also maintained equal to the vertical joint width, i.e. 25 mm. Similarly, the design drift ratios corresponding to sealant tearing for the north elevation panels (with unequal aspect ratios) and the west elevation panels (with equal aspect ratios) are 2.60% and 2.84%, respectively. Detailed design procedures for vertical slot length, horizontal and vertical joint width between panels, steel-embeds for horizontal design actions, and weld-plates for vertical design actions are detailed in Bhatta et al. (2020) and Bhatta, Dhakal, and Sullivan (2023a).

2.2.3. Construction Details and Installation

All the cladding panels were shop-fabricated and reinforced with HD12 rebars spaced at 250 mm in both directions. Once the panels achieved the target compressive strength of 40 MPa, they were transported to the ILEE lab and lifted into place with cranes first at storey 2, followed by storey 3. The vertical alignment of the panels was checked using a laser light, and they were carefully positioned so that the weld-plates (Fig. 6a) rest onto the RHS sections as shown in Fig. 6b. These RHS sections were welded to the beam webs and extended outward. The connection of the cladding panel to the structure was achieved by a bolt in the vertical slot of the steel-embed passing through the horizontal slot in the steel angle, as shown in Fig. 6c,d. The horizontal slots provided in-plane tolerance, allowing for panel adjustment during installation.

A finger-tight nut was applied to the bolt, allowing it to slide freely within the vertical slot. Moreover, horizontal movement of the panels was restrained by tack-welding the nuts to the slotted steel angles at the connections (Fig. 6c). For the cladding panels on the south elevation and the larger panels on the north elevation, tack-welds were applied at two diagonal connections (Refer to Fig. 2b,c

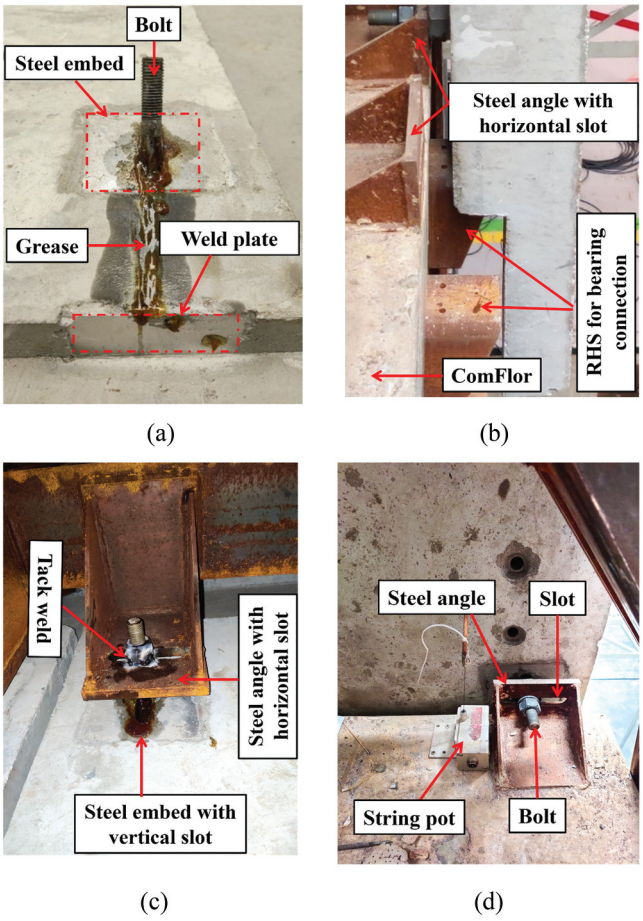

Figure 6. Components of the rocking cladding system: (a) steel-embed and weld-plate; (b) bearing connection; (c) typical tack-welded top connection; (d) typical bottom free connection.

for connection configurations). For all other cladding panels, the two top connections were tack-welded while the bottom connections were left free as depicted in Fig. 6d. These welds were applied without a specific design but were necessary to lock the panels in position and prevent horizontal movement relative to the structure (Bhatta et al. 2020). The vertical and horizontal inter-panel joint gaps were maintained between 20–30 mm wide due to natural installation variation, with an average width of 25 mm. The joints were filled with a one-stage silicone sealant (PCI 2007), which was allowed to cure for three days prior to testing.

3. Test Setup

3.1. Instrumentation Plan

Various sensors were installed to record the response of both the structure and the cladding system. To capture the lateral displacement of each floor, four string potentiometers were mounted at the slab ends on each floor level. In the longitudinal (NS/X) direction, these potentiometers were aligned along the centreline of the structure, while in the transverse (EW/Y) direction, they were positioned along two column lines. Additionally, two uniaxial accelerometers were installed at each floor level (Ground and Levels 1–3) to measure accelerations in the longitudinal (NS/X) and transverse (EW/Y) directions.

A single accelerometer was also mounted at Levels 1, 2, and 3 near the central column to capture vertical (Z-direction) floor accelerations.

The cladding panels were instrumented with potentiometers and uniaxial accelerometers as shown in Fig. 7. The potentiometers measured the panel's uplift, relative horizontal and vertical displacements between adjacent panels, and changes in the vertical joint gap. Vertically oriented

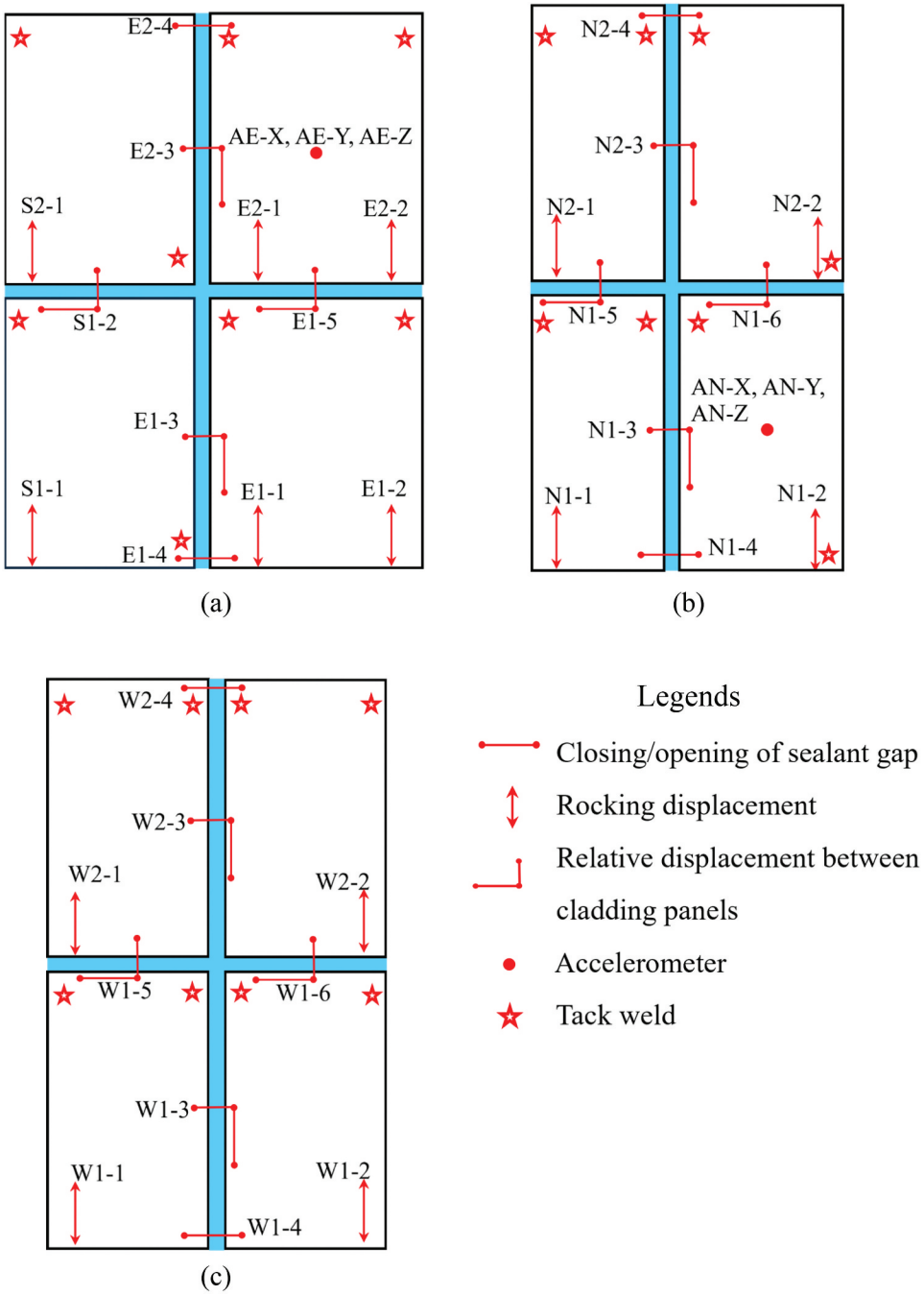

Figure 7. Instrumentation layout for cladding panels: (a) south-east elevation; (b) north elevation; (c) west elevation.

potentiometers recorded panel uplift at the locations where they were attached relative to the composite floor slab. Accelerometers were mounted at the mid-height of the panels to record accelerations in two horizontal directions and one vertical direction. Additionally, horizontal and vertical lines were marked across the sealant joints to visually monitor shear displacements of the sealant.

3.2. Ground Motion and Test Schedule

Shaking during the tests was applied using the El Centro earthquake record. The selection of ground motion was governed by two primary considerations: (i) experimental programme constraints and (ii) suitability of the record for multi-intensity shake table tests. As many structural and non-structural concepts were investigated under the ROBUST research programme, the total number of runs considering multiple ground motions would have resulted in a huge test matrix. This would have imposed constraints on shake table time (mainly due to laboratory arrangements) as well as on overall research funding. Hence, all systems were subjected to one ground motion scaled to multiple intensities to allow comparison across different concepts. Following subjective quantitative assessment for various input shaking scenarios, Imperial Valley, El Centro, 1940, Array #9 station earthquake record was selected, as it provides strong shaking over a wide range of periods and can be scaled to different shaking levels up to the Maximum Considered Earthquake (MCE) within the displacement, velocity, and acceleration capacities of the shake table (Bagheri 2022).

The selected record was scaled to match the target spectrum using NZS 1170.5 (2016). The matching period range of 0.08–1.97 s was selected to cover the full structural configurations. During scaling, the structural performance factor (S_p) and the family scale factor (k_2) were taken as 1.0, while the record scale factor (k_1) was 1.45. This resulted in target peak table accelerations (PTAs) of 0.1 g for Serviceability Limit State (SLS), 0.4 g for Ultimate Limit State (ULS), and 0.73 g for MCE shaking levels. Further details on scaling procedures are provided in Bagheri (2022) and Chan et al. (2026). The testing programme was extended by increasing the intensity gradually from SLS to MCE level (initial goal). As no visible damage was observed at MCE level, the shaking intensity was further increased up to 1.2 × MCE, corresponding to a target PTA of 0.88 g. Table 2 summarises the sequence of tests performed, and their corresponding target input intensities.

The building was tested under unidirectional shaking in both the longitudinal (NS/X) and transverse (EW/Y) directions separately, as well as under bidirectional (XY) input motions. To monitor any variation in dynamic properties such as modal frequencies and damping ratios of the test building as well as non-structural elements, bidirectional (XY) white noise tests were conducted before and following each input ground motion. In addition, intermittent physical inspections of cladding panels, their connections, and sealant joints were conducted throughout the testing to record visible damage, as outlined in Table 2.

4. Experimental Results

Acceleration and displacement data from the shake table tests were recorded at a sampling frequency of 256 Hz. The recorded signals were filtered with a fourth-order Butterworth low-pass filter and 50 Hz cutoff frequency. The filtered datasets were subsequently used to determine the seismic response of the structure and the cladding system, as well as the vibration frequency of the cladding system.

4.1. Peak Seismic Response of Structure

Table 3 presents the peak inter-storey drift ratios (PIDRs) and peak floor accelerations (PFAs) for the building between Levels 1 and 3. PIDRs increased with shaking intensity for both unidirectional (X, Y) and bidirectional (XY) input motions. In the longitudinal (NS/X) direction, the drift response was nearly symmetric between positive and negative drift cycles; therefore, PIDRs were obtained by

Table 2. Loading sequence during NSEs testing in the ROBUST test.

Test number	Intensity	Applied Direction	Target input PTA (g)		Inspection*
			X	Y	
1	SLS	X	0.10	–	
2	SLS	Y	–	0.10	
3	SLS	XY	0.07	0.07	
4	SLS	XY	0.10	0.10	Inspection 1
5	2.0 SLS	X	0.20	–	
6	2.0 SLS	Y	–	0.20	
7	2.0 SLS	XY	0.14	0.14	
8	2.0 SLS	XY	0.20	0.20	Inspection 2
9	3.0 SLS	X	0.30	–	
10	3.0 SLS	Y	–	0.30	
11	3.0 SLS	XY	0.30	0.30	Inspection 3
12	ULS	X	0.40	–	Inspection 4
13	ULS	Y	–	0.40	Inspection 5
14	ULS	XY	0.40	0.40	Inspection 6
15	1.2 ULS	X	0.49	–	Inspection 7
16	1.2 ULS	Y	–	0.49	Inspection 8
17	1.2 ULS	XY	0.49	0.49	Inspection 9
18	1.5 ULS	X	0.60	–	Inspection 10
19	1.5 ULS	Y	–	0.60	
20	1.5 ULS	XY	0.60	0.60	Inspection 11
21	MCE	XY	0.73	0.73	
22	1.2 MCE	XY	0.88	0.88	Inspection 12

*Visual inspections were carried out after respective shaking, and damage observed to specimens was documented.

Table 3. Peak seismic response of the floor levels where cladding panels were installed.

Shaking direction	Target input PTA (g)	Peak floor acceleration, PFA (g)						Peak inter-storey drift ratio, PIDR (%)					
		Long. dir. (NS/X)			Trans. dir. (EW/Y)			Long. dir. (NS/X)		Trans. dir. (EW/Y)			
		Level 1	Level 2	Level 3	Level 1	Level 2	Level 3	Storey 2	Storey 3	Storey 2		Storey 3	
										East	West	East	West
Unidirectional (X, Y)	0.10	0.14	0.13	0.19	0.25	0.20	0.22	0.24	0.17	0.04	−0.05	0.05	−0.03
	0.20	0.36	0.23	0.35	0.33	0.28	0.30	0.51	0.40	0.07	−0.12	0.06	−0.05
	0.30	0.45	0.29	0.40	0.37	0.29	0.34	0.72	0.58	0.07	−0.12	0.06	−0.07
	0.40	0.50	0.38	0.53	0.40	0.35	0.42	1.00	0.87	0.20	−0.18	0.08	−0.07
	0.49	0.59	0.46	0.60	0.56	0.43	0.43	1.16	1.01	0.33	−0.22	0.14	−0.06
	0.60	0.84	0.58	0.68	0.66	0.46	0.48	1.41	1.26	0.52	−0.27	0.29	−0.06
Bidirectional (XY)	0.07	0.13	0.13	0.19	0.29	0.23	0.24	0.20	0.14	0.05	−0.07	0.05	−0.04
	0.10	0.15	0.15	0.20	0.26	0.22	0.24	0.26	0.17	0.05	−0.07	0.04	−0.05
	0.14	0.19	0.18	0.26	0.29	0.24	0.30	0.38	0.23	0.05	−0.07	0.05	−0.05
	0.20	0.35	0.22	0.30	0.26	0.26	0.32	0.45	0.32	0.09	−0.10	0.06	−0.07
	0.30	0.34	0.31	0.43	0.37	0.30	0.37	0.68	0.54	0.16	−0.13	0.08	−0.08
	0.40	0.37	0.33	0.41	0.46	0.40	0.41	0.82	0.68	0.31	−0.20	0.15	−0.07
	0.49	0.50	0.40	0.60	0.55	0.47	0.52	1.13	0.99	0.67	−0.31	0.39	−0.11
	0.60	0.53	0.47	0.67	0.74	0.53	0.61	1.29	1.16	0.93	−0.35	0.65	−0.12
	0.73	0.75	0.57	0.79	0.93	0.60	0.70	1.50	1.33	1.19	−0.41	0.90	−0.13
	0.88	0.80	0.60	0.90	0.95	0.60	0.82	1.71	1.59	1.41	−0.51	1.10	−0.22

averaging the absolute peaks recorded by the two displacement sensors. However, the peaks of the positive (Eastward) and negative (Westward) drift cycles in the transverse (EW/Y) direction differed noticeably after the 0.49 g bidirectional (XY) input. Hence, PIDRs along East and West were obtained by averaging the positive peaks and negative peaks from the displacement sensors, respectively. Across all loading conditions, higher drift ratios were consistently observed in the longitudinal (NS/X) direction compared to the transverse (EW/Y) direction, which can be attributed to the additional lateral stiffness provided by bracing in the transverse direction. Furthermore, PIDRs were greater at the second storey than at the third, with peak values of 1.71% and 1.59% in the longitudinal (NS/X)

direction, and 1.41% and 1.10% in the transverse (EW/Y) direction, respectively. The maximum PIDR of 1.71% occurred on the second storey in the longitudinal (NS/X) direction, which is critical for evaluating the drift demand on the cladding system. The PFAs at each floor level were obtained by averaging the absolute peak accelerations recorded by two accelerometers in each direction. Although PFAs also increased with input ground motion intensity, a consistent amplification trend with building height was not evident. Level 2 often recorded lower PFAs than both Level 1 and Level 3 across all directions and loading types, which could be attributed to the influence of the higher vibrational mode effect. The highest PFA observed was 0.95 g at Level 1 in the transverse (EW/Y) direction, under 0.88 g bidirectional (XY) shaking.

4.2. Seismic Damage

Minor damage was initially observed at a PIDR of 0.51%, characterised by the sealant detachment at the vertical joint between cladding panels E1 and S1 (Fig. 8a). This is an adhesive failure caused by lateral sliding forces in the flat panels during shaking in the longitudinal (NS/X) direction exceeding the adhesive bond strength (Klosowski and Wolf 2016). This was attributed to dust embedded between the sealant and concrete surfaces due to insufficient cleaning, drying, and preparation of the panel edges before sealant application. Such damage was also reported in previous studies by Xue, Tan, and Sha (2020) and Bhatta, Dhakal, and Sullivan (2023a). Wrinkles in the sealant were also first observed at the horizontal joint between panels W1 and W2 at 1.00% PIDR and between panels E1 and E2 at 1.16% PIDR. This response indicates the post-elastic nonlinear behaviour of the sealant when the shear displacement becomes larger. Dal Lago et al. (2017) defined this as the formation of inclined ties, which occurred at 0.90% drift under the cyclic test. Sealant tearing at the vertical joint between the east and south elevation was expected to occur at a PIDR of 1.25%. However, the tearing was not observed because sealant detachment occurred before reaching the expected drift level. For the west and north elevation panels, the maximum PIDR remained below the design drift corresponding to sealant tearing.

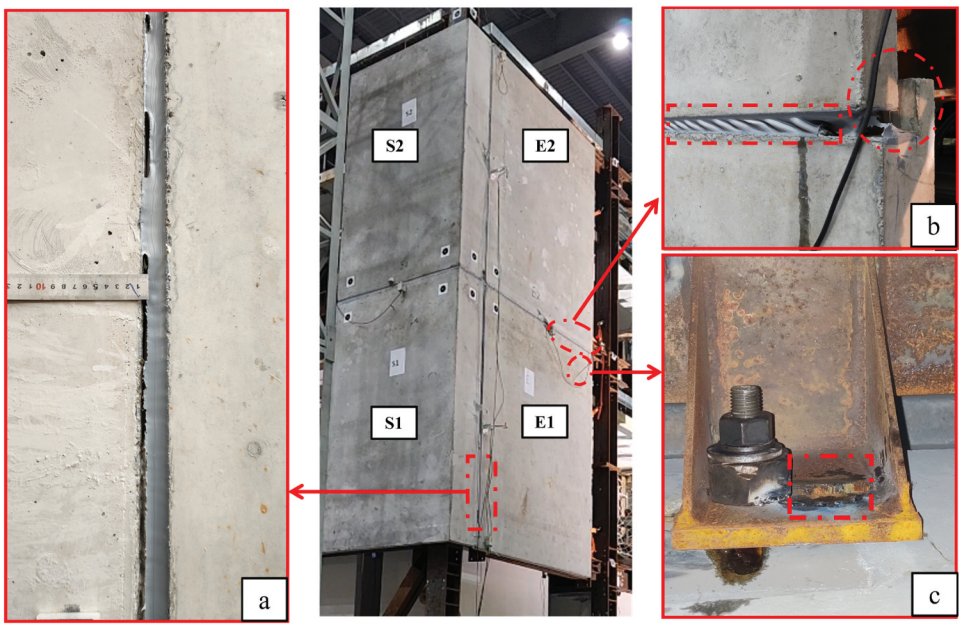

Figure 8. Damage observed in the east elevation cladding panels: (a) sealant detachment at the vertical joint between panels E1 and S1 at 0.51% PIDR (0.20 g shaking in the longitudinal (NS/X) direction); (b) horizontal shifting of cladding panel E1 and appearance of sealant wrinkles after 1.41% PIDR (0.60 g shaking in the longitudinal (NS/X) direction); (c) failure of tack-weld.

With increased shaking intensity, the east elevation panels sustained further damage. On panels E1 and E2, the tack-welded connections between the two top horizontally slotted steel angles and the nuts failed as shown in Fig. 8c during 0.60 g longitudinal direction (NS/X) shaking (PIDRs of 1.41% and 1.26% on the second and third storeys), resulting in horizontal panel movement (Fig. 8b). As these tack-welds were applied without a specific design, their failure was likely due to increased force demands during stronger shaking. Therefore, tack-welds should be designed to resist the required horizontal force in accordance with SNZ TS 1170.5 (2025), considering the specific connection configurations. Such tack-weld failure widened the gap between the east and south elevation panels, leading to the complete detachment of the sealant at the vertical joint. Although this could compromise the weather tightness and thermal insulation of the cladding system, it can be considered as a minor repair damage state since this damage was associated with the failure of the tack-weld. This damage requires repair actions such as repositioning the panels through the slotted steel angles, re-welding the nut-to-plate connections, and resealing the joints. As there was no immediate risk of panel detachment, the test was continued without repairing the specimens, so that a comprehensive evaluation of the performance of the cladding system under extreme seismic conditions could be made.

Additional observations included the breakage and dislodgement of backer rods behind the sealant in the horizontal joints between panels E1 and E2 after 1.16% PIDR. This damage is attributed to repeated panel sliding and the frictional forces developed between the concrete and backer rod, as also reported in a previous study by Bhatta, Dhakal, and Sullivan (2023b). Bolt loosening was also noted during inspections and required retightening to control out-of-plane movement and reduce the risk of panel detachment in subsequent shaking. No other damage, such as loosening and yielding of steel-embeds, cracking, and crushing of panels, was observed during the inspections throughout the test.

4.3. Damage States

The different forms of damage in the cladding system, along with their classification into damage states and the required repair actions, are described in Table 4. The damage states are adapted from the classifications proposed by Bhatta, Cook, and Sattar (2025) and also based on insights from relevant literature (Hutchinson et al. 2014; Pantoli et al. 2016). Table 5 summarises the peak inter-storey drifts at which various damage states were first observed in the cladding system during the experiment.

4.4. Rocking Response of Cladding System

In this section, a comparison is made between the experimental rocking displacements and the theoretically predicted values at various inter-storey drift ratios to evaluate the rocking response of the cladding system. The experimental peak rocking displacement was obtained as the maximum measured uplift at a given shaking level and was plotted against the corresponding peak inter-storey drift ratio. The theoretically predicted rocking displacement was calculated by multiplying the horizontal distance from the bearing connection to the uplift measurement point (instrument location) and the panel rotation, as given by Eq. (1). As the panel height differs from the inter-storey height, the relationship between the panel rotation "δ_p" and inter-storey drift ratio "θ," proposed by Bhatta, Dhakal, and Sullivan (2023a), was adopted:

$$\delta_p = \theta * \frac{H}{h_e} \tag{3}$$

where H is the inter-storey height (3000 mm) and h_e is the height of the steel-embed from the panel bearing point (2575 mm). This relationship was derived for quasi-static drift demands. For cladding systems with diagonal or fully tack-welded connections (i.e. horizontally restrained systems), the response is primarily governed by inter-storey drift rather than acceleration. In systems where only the

Table 4. Definition of damage states and required repair actions (Bhatta, Cook, and Sattar 2025).

Damage state	Description	Required repair action
Superficial	Primarily aesthetic and superficial damage. The structure-to-panel connections remain intact, ensuring that the drift-accommodating mechanism and the system's functionality are maintained. Examples: appearance of wrinkles on the sealant, dislodgment of backer rods.	No immediate repair required.
Minor repair	Minor functionality issues, such as limited water or air leakage, that may require temporary repair but pose no immediate safety risk. Examples: failure of tack-welds, sealant tearing and/or detachment.	Remove damaged sealant, realign panels, re-weld nuts/plates, and reseal the joint.
Major repair	Damage requiring immediate repair, posing a life-safety hazard, and damage irreparably compromising the weather tightness and thermal insulation. Examples: failure of cladding panel-to-structure connections, or cracking/spalling/breaking of cladding panels.	Demolish and replace the affected cladding panel.

Table 5. Summary of the onset of damage states for each specimen.

Damage states	South panel	East panel	North panel	West panel
Superficial	NO*	Appearance of sealant wrinkles at 1.16% PIDR (0.49 g X)**	NO	Appearance of sealant wrinkles at 1.00% PIDR (0.40 g X)
Minor repair	NO	Sealant detachment at 0.51% (0.20 g X) Tack-weld failure at 1.41% and 1.26% PIDR for E1 and E2 panels, respectively (0.60 g X)	NO	NO
Major repair	NO	NO	NO	NO

*NO = Not Observed.
**Numerical values in parentheses indicate the PTA corresponding to the inter-storey drift ratios, and X is the direction of shaking.

top connections are restrained, and the bottom connections are free, the relationship may be considered an upper-bound estimate of drift capacity. Panels in such systems are expected to rock due to the weight of the panels and frictional resistance at the bearing connections. Therefore, the same formulation developed by Bhatta, Dhakal, and Sullivan (2023a) is applicable to the tested specimens to calculate the theoretical rocking values.

4.4.1. Rocking Response of Cladding System with Two Top Tack-Welded Connections

The graph for instrument E2–2 (refer to Fig. 7 for instrument location) shows that the experimental peak rocking displacements closely followed the predicted values, except for the last three data points, which correspond to the phase after tack-weld failure (Fig. 9a). When all four connections were free to slide, the panel did not behave as a completely drift-sensitive element. As a result, the rocking of the cladding panel could have been delayed, i.e. the rocking was accommodated by horizontal sliding and experimental peak rocking displacements were significantly lower than theoretical prediction. However, the lower east elevation panel (E1) continued to rock even after the tack-weld failure, but the rocking was not as much as the predicted values, as shown in the graphs (Fig. 9b) for instrument E2–1 (refer to Fig. 7 for instrument location).

The graph for instrument E1–4 (refer to Fig. 7 for instrument location) shows that the panel E1 did not return to the original position after the tack-weld failure, and the bolts reached near the end of the horizontal slot. The panel permanently shifted by 15 mm at the end of 0.60 g shaking in the longitudinal (NS/X) direction, as shown in Fig. 10a (refer to Fig. 8c for panel position), and the cumulative residual displacement was 31 mm, i.e. this cumulative residual displacement was calculated by summing the residual displacement recorded after each input shaking from the start of the test to a particular shaking. However, the graph for instrument E2–4 (refer to Fig. 7 for instrument location) shows that panel E2 nearly returned to its previous position, leaving a residual displacement of around 3 mm (Fig. 10b), and the cumulative residual displacement was only 5 mm. This indicates that there was sufficient room for the E2 panel to slide sideways. Hence, the rocking of panel E1 was higher since the bolts were near the end of the horizontal slots, acting as shear keys.

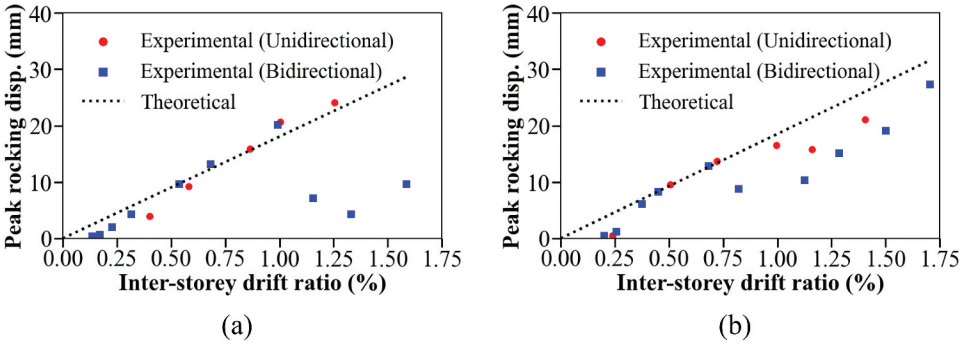

Figure 9. Comparison of experimental and theoretical rocking displacements of east elevation panels at instrumentation points: (a) E2–2; (b) E1–2 (refer to Fig. 7 for instrument locations).

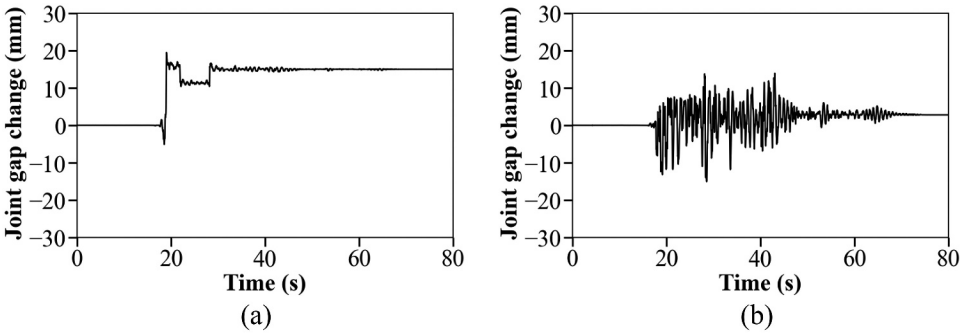

Figure 10. Changes in the vertical joint gap between east and south elevation panels during 0.60 g shaking in the longitudinal (NS/X) direction as recorded by instruments (a) E1–4; (b) E2–4 (refer to Fig. 7 for instrument locations).

The rocking displacement at the free end of the east elevation was greater than at the end adjacent to the south elevation panel. Specifically, the peak rocking displacement measured by instrument E1–2 (located near the free end) exceeded that measured by instrument E1–1 (located near the south elevation panel). This behaviour can be attributed to the boundary conditions at the two ends of the panel. The comparison between instruments E2–1 and E2–2 could not be performed because instrument E2–1 was not working and did not record reliable data. When the panel was subjected to shaking in the direction toward the free end, it was able to slide horizontally until the bolt engaged with the edges of the horizontal slot in the slotted steel angle. In contrast, when shaking was toward the south elevation panel, the available sliding distance was limited to the width of the vertical gap between the south and east elevation panels (ideally, if full compression of the sealant was assumed). Beyond this gap, the panel would come into contact with the adjacent south elevation panel, constraining further sliding and forcing the panel to initiate rocking. Therefore, the panel had more room to slide, and rocking displacements were lower when the shaking direction was toward the free end than toward the south elevation panel.

The experimental results for the west elevation panels (W1 and W2) with equal aspect ratios followed the theoretically predicted rocking line, as shown in Fig. 11. However, the smaller panel on the north elevation (the smallest among all panel configurations) did not exhibit the expected rocking mechanism. The maximum experimental rocking displacement recorded by instruments N1–1 and N2–1 (refer to Fig. 7 for instrument locations) were 2.50 mm and 1.63 mm, respectively, during 0.88 g bidirectional (XY) shaking, whereas the corresponding theoretical rocking displacements were 7.23 mm and 4.86 mm. This deviation can be attributed to the relatively low inter-storey drift ratio

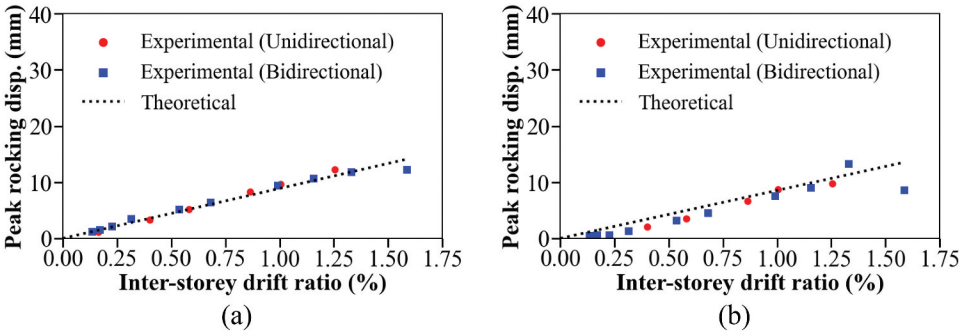

Figure 11. Comparison of experimental and theoretical rocking displacements of west elevation panels at instrumentation points: (a) W2–1; (b) W2–2 (refer to Fig. 7 for instrument locations).

towards the West in the transverse (EW/Y) direction, as shown in Table 3. It should be noted that the drift towards the West induces rocking at the panel end where the instruments were installed. The small drift demand was first mobilised to close the clearance between the vertical slot and the connecting bolt, which might have delayed the engagement of the rocking mechanism and resulted in only partial mobilisation at that location.

4.4.2. Rocking Response of Cladding System with Two Diagonal Tack-Welded Connections

The graphs for rocking displacement of the south elevation panel and the larger panel in the north elevation show that experimental peak rocking displacement closely followed the theoretically predicted values, even at the lower shaking, as shown in Fig. 12. Since the two diagonal connections of these panels were tack-welded, this might have caused them to rock as soon as the loading started, without horizontal sliding.

The experimental peak rocking displacements of other instrumented locations in the panels (not discussed above, see Fig. 7) were also typically smaller than their theoretically predicted values. During and after each shaking, the position of the cladding panels at the bearing connections continuously shifted, albeit by a small amount, due to potential sliding, especially when bottom connections were not tack-welded. As a result, the rocking distance also varied from one shaking event to another. However, the theoretical rocking displacements were calculated using the horizontal distance from the far end of the bearing connection to the instrument location before testing began (initial position). Additionally, the initial positioning of the bolts within the horizontal slots of the steel angle could also influence the rocking response. Due to variations during installation, the initial bolt position could vary significantly. When bolts were positioned near one edge of the horizontal slot, these bolts acted as

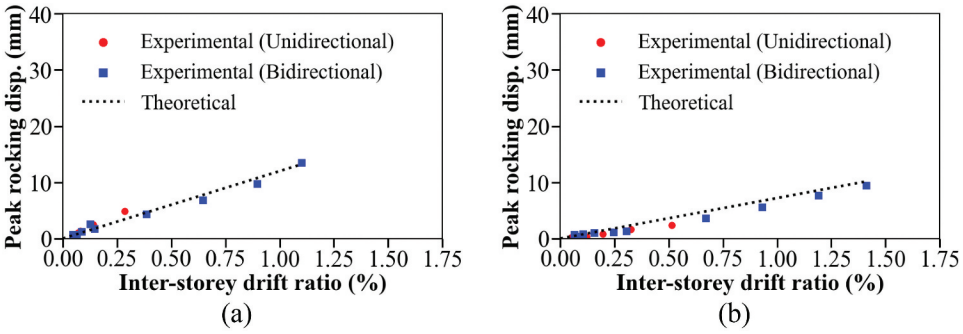

Figure 12. Comparison of experimental and theoretical rocking displacements of panels at instrumentation points: (a) S2–1 at south elevation; (b) N1–2 at north elevation (refer to Fig. 7 for instrument locations).

shear keys, and rocking started immediately, even at small inter-storey drift without sliding. Moreover, the location of cladding panels and the string potentiometers used to calculate the peak inter-storey drift ratios, vibration modes of the structure, and time lag between the occurrence of peak inter-storey drift and peak rocking displacement may also have contributed to the discrepancy between experimental and theoretical rocking displacements.

It is acknowledged that cladding panels installed at adjacent storeys were separated by horizontal joints filled with sealant; therefore, interaction between panels is possible under seismic loading. In addition, the PIDRs along the transverse (EW/Y) direction in Storey 2 and Storey 3 show significant differences (Table 3) especially after the 0.4 g shaking. It can be argued that a panel with larger rocking rotation may induce additional rotation in an adjacent panel if the available joint gap is insufficient, or if any geometric constraints prevent relative movement. To evaluate whether such a mechanism could have occurred, the peak rocking displacements of the south elevation panels (the largest panels in the transverse direction) in the two storeys were compared throughout the tests. The maximum difference in peak rocking displacement between the Storey 2 and Storey 3 panels was approximately 10 mm during the 0.88 g bidirectional shaking, which is smaller than the available horizontal joint gap of approximately 30 mm. Therefore, the results suggest that interaction due to geometric constraints is unlikely to have occurred in the present test configuration. Furthermore, the Storey 3 panels exhibited peak rocking displacements lower than the theoretical response line, indicating independent rocking without any rotation imposed by the Storey 2 panels. However, the interaction mechanism described above could be critical in certain scenarios; for example, if a panel fails to rock due to an installation error, or if adjacent panels rock in opposite directions in tall structures undergoing higher mode response. In such cases, careful consideration should be given to the maximum allowable uplift and the corresponding joint widths between panels to avoid such interaction.

4.5. Relative Displacement Between Cladding Panels

Table 6 shows that the peak and cumulative residual values of relative horizontal displacement, changes in the vertical joint gap, and relative vertical displacement are minimum for the panels with diagonally tack-welded connections. Relative horizontal displacement refers to lateral sliding between the top and bottom panels, while changes in the vertical joint gap indicate the opening or closing of the vertical gap between adjacent panels within the same storey. Relative vertical displacement denotes the difference in vertical movement between adjacent panels during rocking motion. Peak displacements for each instrument were taken as the maximum displacement recorded throughout the tests, while cumulative residual displacements were calculated by summing the residual displacements recorded by each instrument after each input shaking, from the start of the test to the final event. For panels with two

Table 6. Peak displacement and cumulative residual displacement.

Relative horizontal displacement						
Instrument notation	E1–5	W1–5	W1–6	S1–2	N1–5	N1–6
Peak displacement (mm)	49.61	52.91	60.73	9.88	8.16	5.78
Cumulative residual displacement (mm)	38.97	13.75	7.93	−3.67	4.81	7.49
Changes in the vertical joint gap						
Instrument notation	E1–4	E2–4	W1–4	W2–4	N1–4	N2–4
Peak displacement (mm)	19.46	39.41	8.67	6.29	3.20	2.41
Cumulative residual displacement (mm)	46.09	15.29	−2.33	−0.38	0.59	−0.14
Relative vertical displacement						
Instrument notation	E1–3	E2–3	W1–3	W2–3	N1–3	N2–3
Peak displacement (mm)	16.88	21.94	27.48	21.84	9.12	5.58
Cumulative residual displacement (mm)	9.63	4.46	−7.84	−0.30	−1.13	0.14

top connections tack-welded while the bottom connections remained free, the cumulative residual displacement for changes in the vertical joint gap was smaller at the top of the panels than at the bottom, i.e. E2–4 < E1–4 and W2–4 < W1–4 (refer to Fig. 7 for instrument locations).

4.6. Component Acceleration Amplification Factor

Since the cladding panels were connected at two levels, the acceleration amplification measured at the top and bottom connections can vary. Therefore, a single value of the acceleration amplification factor may not represent the overall amplification of the cladding system. In this study, the component acceleration amplification factor was calculated by normalising the peak acceleration measured at the mid-height of the cladding panel by the peak acceleration of the supporting floor (either the top or bottom level). For example, the in-plane bottom and in-plane top amplification factors, referred to as IPA (bot) and IPA (top), respectively, for the east elevation panel were calculated by dividing the panel acceleration in the longitudinal (NS/X) direction by the corresponding peak floor accelerations at Levels 2 and 3, as shown in Fig. 13a. Before the tack-weld failure, the median IPA (bot) and IPA (top) were 2.54 and 1.94, respectively, and these values decreased to 2.14 and 1.50 after the failure. Conversely, the out-of-plane amplification (OPA) factor shows no significant change before and after tack-weld failure, with median OPA values of 1.65 (bot) and 1.48 (top). The amplification factors for the north elevation panel (with two diagonal tack-welded connections), as shown in Fig. 13b, were determined using the same procedure described above. The median IPA (bot) and IPA (top) were 0.75 and 0.86, while the median OPA (bot) and OPA (top) were 0.91 and 1.08, respectively. The results indicate that the component acceleration amplification factors were lower for the panels with two diagonally tack-welded connections than with two top tack-welded connections. The lower acceleration amplification values can be attributed to the lower impact forces, as both the panel weight and rocking displacements were small for the north elevation panels. The experimental findings for the cladding system with two top tack-welded connections in the present study align with previous studies showing higher in-plane amplification than out-of-plane amplification in cladding systems (Huang, Lu, and Mosalam 2018; Kamau-Devers 2016).

The reduction in acceleration amplification for the east elevation panel after tack-weld failure is attributed to decreased rocking motion after the failure, which reduced impact forces and the corresponding peak panel accelerations. Figure 14 presents the in-plane and vertical acceleration time histories of the east elevation panel during 0.49 g shaking in the longitudinal (NS/X) direction, clearly illustrating the impact effects.

For the cladding system with two diagonal tack-welded connections (north elevation), the median amplification factors were generally less than unity (median values 0.75–1.08). Therefore, the ASCE/SEI 7-22 (2022) provision of 1.0 may be conservative for this connection configuration. According to SNZ TS 1170.5 (2025), the amplification factors calculated in the present study correspond to the ratio

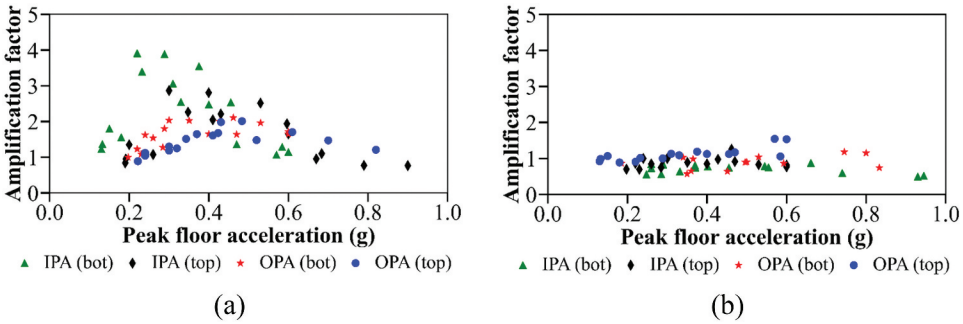

Figure 13. Component acceleration amplification factors: (a) east elevation panel; (b) north elevation panel.

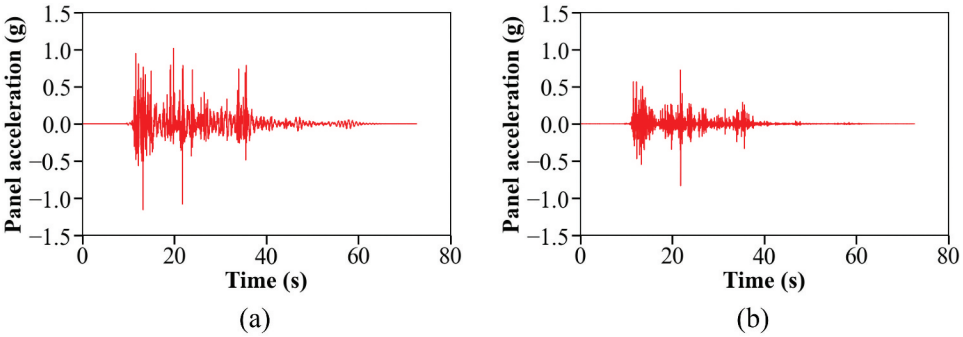

Figure 14. East elevation panel acceleration time histories: (a) AE–X; (b) AE–Z.

$C_i(T_p)/C_{ph}$ for various ductility levels (μ) where $C_i(T_p)$ is the component spectral-shape coefficient and C_{ph} is the component-horizontal-response factor. With no noticeable amplification, the cladding systems with two diagonal tack-welded connections behave like rigid-components as per the definition in SNZ TS 1170.5 (2025). In contrast, the cladding system with two top tack-welded connections (east elevation) exhibited significantly higher amplification factors, with median values ranging from 1.48 to 2.54. These values exceed both the ASCE/SEI 7-22 (2022) factor of 1 and SNZ TS 1170.5 (2025) factor of 1.43 (for $\mu = 2$), suggesting that current code provisions underestimate the amplification factors for this connection configuration. Furthermore, the experimental results suggest that the connection configuration of the cladding system influences component acceleration amplification. The amplification factors also varied between the upper and lower floors. These findings highlight the need for updated design guidelines that account for dynamic behaviour, particularly for newly developed rocking cladding systems. For design purposes, amplification factors for rocking cladding systems may be selected based on connection detailing. The amplification factor for the cladding system with two diagonal tack-welded connections may conservatively be taken as 1.0. In contrast, for the cladding system with two top tack-welded connections, the design amplification factor may conservatively be taken as 2.5 with respect to the lower floor, as the median amplification factors calculated were higher for bottom floors.

It is acknowledged that although the tests did not include vertical inputs, the rocking of the cladding panels generated noticeable vertical accelerations in the panels. The east and north elevation panels recorded peak vertical accelerations of up to 0.87 g (AE–Z) and 0.61 g (AN–Z), respectively, whereas the vertical peak floor acceleration of Level 1 and Level 2 were 1.11 g and 0.22 g, respectively. The high vertical peak floor acceleration may be attributed to impact, which requires further investigation.

4.7. Vibration Frequency

The vibration frequencies of the cladding system were identified through Frequency Response Functions (FRFs). These FRFs were obtained by calculating the ratio of Fourier Transform (FT) amplitudes of accelerations recorded on the cladding panels at various locations (shown in Fig. 7) to the FT amplitudes of the supporting floor accelerations recorded in the same direction during white noise tests. In cases where the FRF results were less conclusive due to the absence of distinct peaks relative to the supporting floors or when a peak was observed with respect to only one floor, the FT was used for verification. Peaks were confirmed when the panel acceleration amplitudes were higher than those of both supporting floors, following the procedure adopted by Pantoli and Hutchinson (2015).

4.7.1. North Elevation Panel (Two Diagonal Tack-Welded Connections)

Figure 15a presents representative FT and FRF of the vertical accelerometer (AN–Z) and out-of-plane accelerometer (AN–X); refer to Fig. 7 for instrument location, on the north elevation panel. The peaks in FRFs of vertical accelerations of both Level 1 and Level 2 are closely spaced within the 3–5 Hz

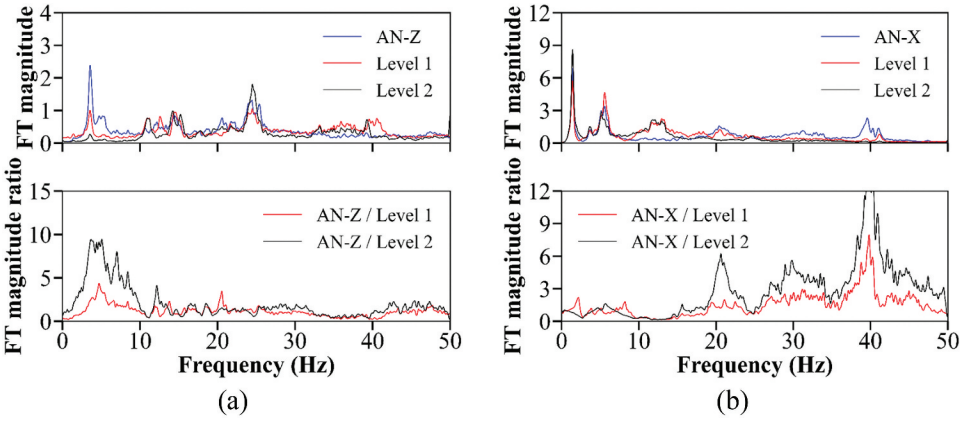

Figure 15. Representative FT and FRF of the acceleration signal of cladding panels on the north elevation: (a) vertical direction; (b) out-of-plane direction.

frequency range, with the first peak occurring at 3.82 Hz at the start of the test. This vibration frequency can be considered as representative of the rocking mode vibration. The multiple peaks observed in these functions suggest that multiple vibration modes contributed to the response of the cladding system. Similarly, the FRF of the out-of-plane acceleration shows peak was observed at 20.95 Hz at the start of the test (Fig. 15b). Along the in-plane direction (AN–Y; refer to Fig. 7 for instrument location), the vibration frequency could not be determined from the FRF results. The FT magnitude also falls between those of the top and bottom floor responses across all frequency ranges in all white noise cases.

Figure 16 summarises the variation of the vibration frequencies of cladding system with two diagonal tack-welded connections along the vertical and out-of-plane horizontal direction with the white noise cases. There is no significant variation in these frequencies across tests, suggesting that no damage occurred to the north elevation cladding panel or its connections. Overall, the vibration frequencies of the such cladding system ranged approximately from 3.57 Hz to 3.84 Hz (0.28 s to 0.26 s) in the vertical direction, and from 19.09 Hz to 21.67 Hz (0.05 s to 0.04 s) in the out-of-plane direction.

4.7.2. East Elevation Panel (Two Top Tack-Welded Connections)

Figure 17a shows that the peaks were observed in the FRF of vertical acceleration of the east elevation panel with respect to both the floors. Along the in-plane direction (AE–X; refer to Fig. 7 for instrument

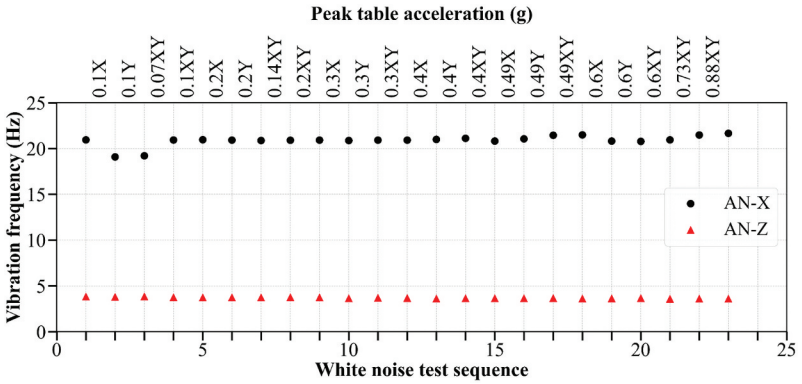

Figure 16. Variation of vibration frequencies of the north elevation cladding panels across white noise tests. Peak table accelerations of the shaking sequence, after which white noise tests were conducted, have also been shown along the top horizontal axis.

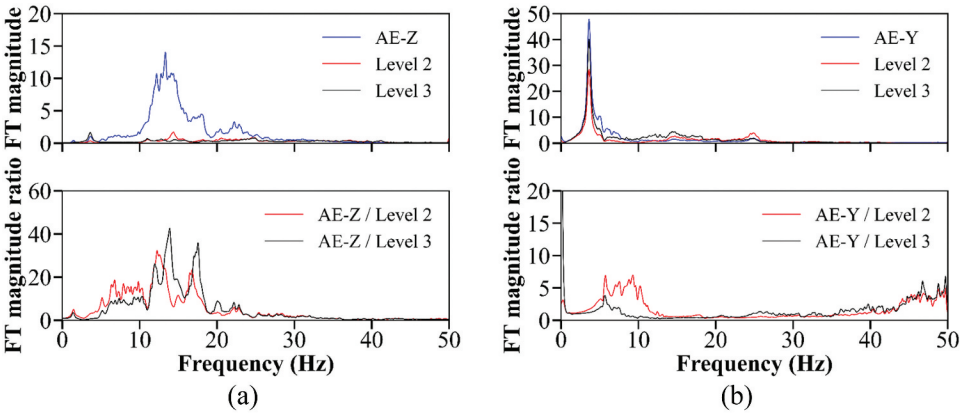

Figure 17. Representative FT and FRF of the acceleration signal of cladding panels on the east elevation: (a) vertical direction; (b) out-of-plane direction.

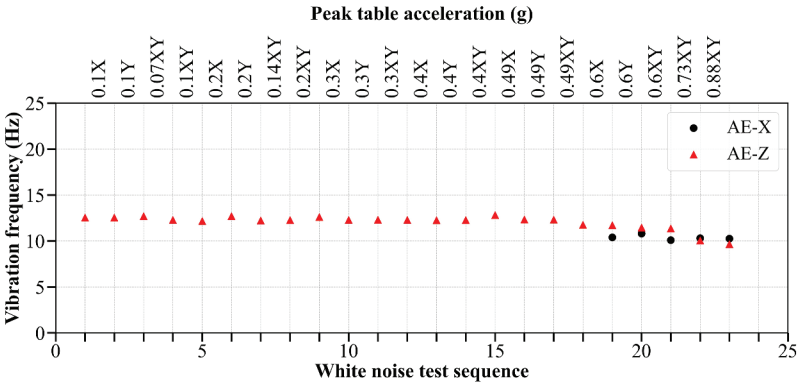

Figure 18. Variation of vibration frequencies of the east elevation cladding panels across white noise tests. Peak table accelerations of the shaking sequence, after which white noise tests were conducted, have also been shown along the horizontal top axis.

location), no clear peaks were identified during the initial white noise tests. After the 0.30 g shaking in the longitudinal (NS/X) direction, the first noticeable peak appeared at 11.88 Hz in FT only and became more pronounced in FRF when the tack-weld failure occurred. However, in the out-of-plane direction (AE–Y; refer to Fig. 7 for the instrument location), the FRF results are less conclusive, as the panel acceleration signal peaks were continuously changing and amplification peaks could not be clearly identified (Fig. 17b).

The vibration frequency of cladding system with two top tack-welded connections, along the vertical and in-plane horizontal direction, ranged from 9.65 Hz to 12.82 Hz (0.10 s to 0.08 s) and 10.10 Hz to 10.80 Hz (0.10 s to 0.09 s), respectively as shown in Fig. 18. The results indicate that the vibration frequency decreased due to the initiation of damage in the cladding connection system.

5. Conclusions

Full-scale shake table tests were conducted on a three-storey steel frame building, subjected to both unidirectional (X, Y) and bidirectional (XY) horizontal shaking. A total of twelve rocking precast concrete cladding panels, each comprising of four vertical sliding connections and two bearing connections were installed on the upper two storeys. The experimental results show that the cladding

systems experienced peak inter-storey drift ratios of up to 1.71% and horizontal peak floor accelerations of up to 0.95 g. The following conclusions can be drawn based on the analysis of the experimental data and observed damage during the shake table tests:

(1) The rocking precast concrete cladding system experienced minor damage throughout the testing programme. Damage to the sealant was first observed at a peak inter-storey drift ratio of 0.51% in one of the cladding systems, which was attributed to inadequate surface preparation, leading to adhesion failure. Tack-weld failure was observed in only two out of the twelve panels (E1 and E2) at peak inter-storey drift ratios of 1.41% and 1.26%, respectively. Despite these issues, all panels performed well under both unidirectional and bidirectional shaking with no severe damage or collapse, demonstrating vertical sliding connections as a low-damage solution for cladding systems in earthquake-prone regions.
(2) The measured peak rocking displacements were generally consistent with the predicted displacements, except for a few of the cladding panels. The experimental results show that the panels with two diagonally tack-welded connections performed better than those with the two top connections tack-welded.
(3) The experimentally derived component acceleration amplification factors for the cladding system with two diagonally tack-welded connections exhibited comparatively low values (median range 0.75–1.1), whereas the cladding system with two top tack-welded connections exhibited moderate amplification (median range 1.5–2.5). These findings demonstrate that connection detailing can influence component acceleration amplification.
(4) The vibration frequency peaks were distinctly visible in the vertical direction. The cladding panels with two diagonal tack-welded connections exhibited rocking mode frequencies ranging approximately from 3.57 Hz to 3.84 Hz (0.28 s to 0.26 s), whereas cladding panels with two top tack-welded connections showed higher rocking frequencies between 9.65 Hz and 12.82 Hz (0.10 s to 0.08 s).

It is acknowledged that the present study focused on evaluating the seismic response of the rocking cladding system primarily under horizontal seismic excitation, and the influence of vertical seismic inputs was not considered within the experimental scope. Nevertheless, vertical ground motions may further influence the overall response of rocking cladding systems to some extent. Therefore, future research incorporating combined horizontal and vertical seismic excitation, supported by numerical analyses considering these effects, would be beneficial in improving the understanding of the seismic behaviour of such cladding panels with vertical sliding connections.

Acknowledgments

The work described was conducted as part of a joint NZ-China research program with the International Laboratories on Earthquake Engineering (ILEE), Tongji University, Shanghai, China and directly with Tongji University, Shanghai, China. Direct NZ funding is kindly provided by the Building Research Association of NZ (BRANZ) under the Building Research Levy, Natural Hazards Commission Toka Tū Ake (formerly known as the Earthquake Commission, EQC), the HERA Foundation (a charitable trust associated with the Heavy Engineering Research Association), the Building Innovation Partnership, the Tertiary Education Commission funded QuakeCoRE (the NZ ILEE partner through whom the NZ funding is also coordinated), the University of Auckland (UA) and Auckland University of Technology (AUT) through the NZ Ministry of Business, Innovation and Employment (MBIE) Endeavour Programme on Sustainable Earthquake Resilient Buildings for a Better Future - PROP-83779-ENDRP-AUT). Administrative and personnel support is also provided by the University of Canterbury (UC). Donations of materials are provided by ComFlor, Hilti Corporation, Tracklok, Gripple, Lanyon & LeCompte Construction Ltd., and Alutech Doors & Windows Ltd. Expertise has been generously provided by a number of Chinese and NZ industry representatives. The authors gratefully acknowledge this support. Opinions expressed are those of the authors alone. The QuakeCoRE paper number is 1117.

Author Contributions

CRediT: **R. K. Shrestha:** Conceptualization, Data curation, Formal analysis, Investigation, Methodology, Validation, Visualization, Writing – original draft, Writing – review & editing; **J. Bhatta:** Conceptualization, Methodology, Resources, Supervision, Writing – review & editing; **R. P. Dhakal:** Conceptualization, Funding acquisition, Project administration, Resources, Supervision, Writing – review & editing; **T. J. Sullivan:** Supervision, Writing – review & editing; **A. Tiwari:** Investigation, Writing – review & editing; **Z. Yan:** Investigation, Project administration, Writing – review & editing; **G. A. MacRae:** Funding acquisition, Project administration, Writing – review & editing; **Y. Zhang:** Investigation, Writing – review & editing; **Z. Li:** Investigation, Writing – review & editing; **P. Xiang:** Funding acquisition, Project administration, Writing – review & editing; **L. J. Jia:** Funding acquisition, Project administration, Writing – review & editing; **S. Ramhormozian:** Funding acquisition, Project administration, Writing – review & editing; **G. C. Clifton:** Funding acquisition, Project administration, Writing – review & editing; **P. Quenneville:** Funding acquisition, Project administration, Writing – review & editing; **G. Rodgers:** Funding acquisition, Project administration, Writing – review & editing; **X. Zhao:** Funding acquisition, Project administration.

Disclosure Statement

No potential conflict of interest was reported by the author(s).

ORCID

R. P. Dhakal http://orcid.org/0000-0001-5524-5919

Data Availability Statement

The data that support the findings of this study are openly available in figshare at https://doi.org/10.6084/m9.figshare.31970820.

References

ASCE/SEI 7-10. 2010. "Minimum Design Loads for Buildings and Other Structures." Reston, Virginia: American Society of Civil Engineers.

ASCE/SEI 7-22. 2022. "Minimum Design Loads and Associated Criteria for Buildings and Other Structures." Reston, Virginia: American Society of Civil Engineers. https://doi.org/10.1061/9780784415788.

Bagheri, H. 2022. "Seismic Performance of a Full-Scale Steel Structure Using Resilient Slip Friction Joints." PhD Dissertation, Department of Civil and Environmental Engineering, University of Auckland. https://hdl.handle.net/2292/60019.

Baird, A. 2014. "Seismic Performance of Precast Concrete Cladding Systems." PhD Dissertation, Civil and Natural Resources Engineering, University of Canterbury. https://doi.org/10.26021/2533.

Baird, A., and H. Ferner. 2017. "Damage to Non-Structural Elements in the 2016 Kaikōura Earthquake." *Bulletin of the New Zealand Society for Earthquake Engineering* 50 (2): 187–193. https://doi.org/10.5459/bnzsee.50.2.187-193.

Baird, A., A. Palermo, and S. Pampanin. 2011. "Facade Damage Assessment of Multi-Storey Buildings in the 2011 Christchurch Earthquake." *Bulletin of the New Zealand Society for Earthquake Engineering* 44 (4): 368–376. https://doi.org/10.5459/bnzsee.44.4.368-376.

Baird, A., A. S. Tasligedik, A. Palermo, and S. Pampanin. 2014. "Seismic Performance of Vertical Nonstructural Components in the 22 February 2011 Christchurch Earthquake." *Earthquake Spectra* 30 (1): 401–425. https://doi.org/10.1193/031013EQS067M.

Bhatta, J., D. T. Cook, and S. Sattar. 2025. "Development of Full-scale Experiment-based Seismic Fragility Functions for Code-compliant Fire Sprinkler Piping Systems." *Earthquake Spectra (Recently accepted)*. https://doi.org/10.1002/esp4.70085.

Bhatta, J., R. P. Dhakal, and T. J. Sullivan. 2023a. "Cyclic Behaviour of Two-Story Low-Damage Rocking Precast Concrete Cladding Panel System." *Journal of Earthquake Engineering* 27 (6): 1414–1439. https://doi.org/10.1080/13632469.2022.2074918.

Bhatta, J., R. P. Dhakal, and T. J. Sullivan. 2023b. "Seismic Performance of a Rocking Precast Concrete Cladding Panel System Under Lateral Cyclic Displacement Demands." *Journal of Earthquake Engineering* 27 (4): 929–958. https://doi.org/10.1080/13632469.2022.2033359.

Bhatta, J., R. P. Dhakal, T. J. Sullivan, and M. Lanyon. 2020. "Low-Damage Rocking Precast Concrete Cladding Panels: Design Approach and Experimental Validation." *Journal of Earthquake Engineering* 26 (9): 4387–4420. https://doi.org/10.1080/13632469.2020.1830201.

Bianchi, S., J. Ciurlanti, D. Perrone, A. Filiatrault, A. C. Costa, P. X. Candeias, A. A. Correia, and S. Pampanin. 2021. "Shake-Table Tests of Innovative Drift Sensitive Nonstructural Elements in a Low-Damage Structural System." *Earthquake Engineering and Structural Dynamics* 50 (9): 2398–2420. https://doi.org/10.1002/eqe.3452.

Bournas, D. A., P. Negro, and F. F. Taucer. 2014. "Performance of Industrial Buildings During the Emilia Earthquakes in Northern Italy and Recommendations for Their Strengthening." *Bulletin of Earthquake Engineering* 12 (5): 2383–2404. https://doi.org/10.1007/s10518-013-9466-z.

Bradley, B. A., R. P. Dhakal, M. Cubrinovski, G. A. MacRae, and D. S. Lee. 2009. "Seismic Loss Estimation for Efficient Decision Making." *Bulletin of the New Zealand Society for Earthquake Engineering* 42 (2): 96–110. https://doi.org/10.5459/bnzsee.42.2.96-110.

Chan, N., A. Hashemi, S. Assadi, B. Hamed, C. Clifton, G. MacRae, R. Dhakal, L.J. Jia, and P. Quenneville. 2026. "Shake Table Tests of a Three-Story Steel Structure with RSFJ." *Journal of Structural Engineering* 152 (4): 4026025. https://doi.org/10.1061/JSENDH.STENG-14988.

Dal Lago, B., F. Biondini, G. Toniolo, and M. Lamperti Tornaghi. 2017. "Experimental Investigation on the Influence of Silicone Sealant on the Seismic Behaviour of Precast Facades." *Bulletin of Earthquake Engineering* 15 (4): 1771–1787. https://doi.org/10.1007/s10518-016-0045-y.

Dhakal, R. P. 2010. "Damage to Non-Structural Components and Contents in 2010 Darfield Earthquake." *Bulletin of the New Zealand Society for Earthquake Engineering* 43 (4): 404–411. https://doi.org/10.5459/bnzsee.43.4.404-411.

Dhakal, R. P. 2024. "Seismic Design of Buildings: Where to Next?" *Bulletin of the New Zealand Society for Earthquake Engineering* 57 (1): 1–17. https://doi.org/10.5459/bnzsee.1680.

Dhakal, R. P., J. B. Mander, and L. Xu. 2010. "Seismic Financial Loss Estimation of Steel Moment Frame Buildings." *International Review of Civil Engineering* 1 (2): 130–142.

Dhakal, R. P., A. Pourali, A. S. Tasligedik, T. Yeow, A. Baird, G. MacRae, S. Pampanin, and A. Palermo. 2016. "Seismic Performance of Non-Structural Components and Contents in Buildings: An Overview of NZ Research." *Earthquake Engineering and Engineering Vibration* 15 (1): 1–17. https://doi.org/10.1007/s11803-016-0301-9.

Dhakal, R. P., M. Rashid, J. Bhatta, C. Chen, G. Q. Song, T. J. Sullivan, G. A. MacRae, G. C. Clifton, P. Xiang, and L. J. Jia. 2020. "Shake Table Testing Plan for Multiple Non-Structural Elements & Contents in a Low–Damage Structural Steel Building." In *17th World Conference on Earthquake Engineering, 17WCEE*, Sendai, Japan, September, 2020, C001122. https://hdl.handle.net/10092/102619.

FEMA-74. 2011. "Reducing the Risks of Nonstructural Earthquake Damage – A Practical Guide." Washington, DC: Federal Emergency Management Agency.

Filiatrault, A., and T. Sullivan. 2014. "Performance-Based Seismic Design of Nonstructural Building Components: The Next Frontier of Earthquake Engineering." *Earthquake Engineering and Engineering Vibration* 13 (1): 17–46. https://doi.org/10.1007/s11803-014-0238-9.

Haymes, K., T. J. Sullivan, and J. Hare. 2025. "Recommendations for the Revision of the Approach for Seismic Design of Parts and Components in New Zealand Design Standards." *Bulletin of the New Zealand Society for Earthquake Engineering* 58 (1 SE–Articles): 52–72. https://doi.org/10.5459/bnzsee.1661.

Huang, B., W. Lu, and K. M. Mosalam. 2018. "Shaking Table Testing of Granite Cladding with Undercut Bolt Anchorage." *Engineering Structures* 171:488–499. https://doi.org/10.1016/J.ENGSTRUCT.2018.05.116.

Hutchinson, T., E. Pantoli, K. McMullin, M. Hildebrand, and G. Underwood. 2014. "Seismic Drift Compatibility of Architectural Precast Concrete Panels and Connections: A Design Guide for Engineers." San Diego: Department of Structural engineering, University of California.

Kamau-Devers, K. C. 2016. "Data Reduction of a Shake-Table Experimental Study of Architectural Precast Concrete Cladding." Master's Theses, San Jose State University. https://doi.org/10.31979/etd.6g5a-3njg.

Khakurel, S., R. P. Dhakal, T. Z. Yeow, and S. K. Saha. 2020. "Performance Group Weighting Factors for Rapid Seismic Loss Estimation of Buildings of Different Usage." *Earthquake Spectra* 36 (3): 1141–1165. https://doi.org/10.1177/8755293019901311.

Klosowski, J., and A. T. Wolf. 2016. *Sealants in Construction*. 2nd ed. Boca Raton: CRC Press. https://doi.org/10.1201/b18995.

Lam, N., and E. Gad. 2002. "An Innovative Approach to the Seismic Assessment of Non-Structural Components in Buildings." In *Australian Earthquake Engineering Society Conference: Total Risk Management in the Privatised Era AEES 2002*, Adelaide, Australia, October 2002, 10. https://doi.org/10.25916/sut.26289874.

MacRae, G., L.J. Jia, Z. Yan, C. Clifton, S. Ramhormozian, R. Dhakal, P. Xiang, G. Rodgers, P. Quenneville, and X. Zhao. 2024. "The Robust Steel Building Response." In *NZSEE 2024 Annual Conference*, Wellington, New Zealand, April, 2024, 147.

MacRae, G., X. Zhao, L. Jia, G. Clifton, R. Dhakal, P. Xiang, S. Ramhormozian, and G. Rodgers. 2020. "The China-NZ ROBUST Friction Building Shaking Table Testing Overview." In *The 17th World Conference on Earthquake Engineering*, Sendai, Japan, September, 2020, 2g–0044. https://ir.canterbury.ac.nz/bitstreams/91612e40-fe1c-4336-bf25-f515416a4686/download.

McMullin, K. M., M. Ortiz, L. Patel, S. Yarra, T. Kishimoto, C. Stewart, and B. Steed. 2012. "Response of Exterior Precast Concrete Cladding Panels in NEES-TIPS/NEESgc/E-Defense Tests on a Full Scale 5-Story Building." Structures Congress, Chicago, Illinois, United States, March, 2012, 1305–1314. https://doi.org/10.1061/9780784412367.117.

Merrick, D., K. McMullin, M. Hildebrand, and A. Kwong. 2003. "In-Situ Vibration Characteristics of Precast Cladding Panels." In *Engineering Smarter: Proceedings of the 2003 Structures Congress and Exposition*, Seattle, Washington, May, 2003.

Miranda, E., G. Mosqueda, R. Retamales, and G. Pekcan. 2012. "Performance of Nonstructural Components During the 27 February 2010 Chile Earthquake." *Earthquake Spectra* 28 (1_suppl1): 453–471. https://doi.org/10.1193/1.4000032.

NZS 1170.0. 2002. Structural Design Actions: General Principles. Standards New Zealand.

NZS 1170.5. 2016. Structural Design Actions: Earthquake Actions. Standards New Zealand.

O'Reilly, G. J., D. Perrone, M. Fox, R. Monteiro, and A. Filiatrault. 2018. "Seismic Assessment and Loss Estimation of Existing School Buildings in Italy." *Engineering Structures* 168:142–162. https://doi.org/10.1016/j.engstruct.2018.04.056.

Pantoli, E., M. C. Chen, X. Wang, R. Astroza, H. Ebrahimian, T. C. Hutchinson, J. P. Conte, et al. 2016. "Full-Scale Structural and Nonstructural Building System Performance During Earthquakes: Part II - NCS Damage States." *Earthquake Spectra* 32 (2): 771–794. https://doi.org/10.1193/012414EQS017M.

Pantoli, E., M. Chen, T. Hutchinson, G. A. Underwood, and M. Hildebrand. 2013. "Shake Table Testing of a Full-Scale Five-Story Building: Seismic Performance of Precast Concrete Cladding Panels." In 4th International Conference on Computational Methods in Structural Dynamics and Earthquake Engineering, 12-14 June 2013, Kos Island, Greece, 1569–1587. https://doi.org/10.7712/120113.4616.C1573.

Pantoli, E., and T. Hutchinson. 2019. "Seismic Accelerations in Architectural Precast Concrete Cladding." *Engineering Structures* 180:742–749. https://doi.org/10.1016/J.ENGSTRUCT.2018.11.062.

Pantoli, E., and T.C. Hutchinson. 2015. "Experimental and Analytical Study of the Dynamic Characteristics of Architectural Precast Concrete Cladding." In Improving the Seismic Performance of Existing Buildings and Other Structures, San Francisco, California, December, 2015, 560–574. https://doi.org/10.1061/9780784479728.046.

PCI. 2007. *Architectural Precast Concrete*. Chicago: Precast/Prestressed Concrete Institute.

Rashid, M., R. Dhakal, and T. Sullivan. 2021. "Seismic Design of Acceleration-Sensitive Non-Structural Elements in New Zealand: State-of-Practice and Recommended Changes." *Bulletin of the New Zealand Society for Earthquake Engineering* 54 (4 SE–Articles): 243–262. https://doi.org/10.5459/bnzsee.54.4.243-262.

Rihal, S. S. 1988. "Seismic Behavior and Design of Precast Facades / Claddings & Connections in Low / Medium-Rise Buildings." San Luis Obispo, California: California Polytechnic State University.

Sagbas, G., R. Sheikhi Garjan, K. Sarikaya, and D. Deniz. 2024. "Field Reconnaissance on Seismic Performance and Functionality of Turkish Industrial Facilities Affected by the 2023 Kahramanmaras Earthquake Sequence." *Bulletin of Earthquake Engineering* 22 (1): 227–254. https://doi.org/10.1007/s10518-023-01741-8.

SNZ TS 1170.5. 2025. Structural Design Actions Part 5: Earthquake Actions. Standards New Zealand.

Steel & Tube Ltd. 2016. "ComFlor 80 Composite Floor Decking." https://steelandtube.co.nz/sites/default/files/catalogues/Comflor80_PG-Dec2016-01.pdf.

Taghavi, S., and E. Miranda. 2003. Response Assessment of Nonstructural Building Elements. Berkeley, CA: The Pacific Earthquake Engineering Research Center.

Toniolo, G., and A. Colombo. 2012. "Precast Concrete Structures: The Lessons Learned from the L'Aquila Earthquake." *Structural Concrete* 13 (2): 73–83. https://doi.org/10.1002/suco.201100052.

Villaverde, R. 1997. "Seismic Design of Secondary Structures: State of the Art." *Journal of Structural Engineering* 123 (8). https://doi.org/10.1061/(ASCE)0733-9445(1997)123:8(1011).

Wang, M. L. 1987. "Cladding Performance on a Full Scale Test Frame." *Earthquake Spectra* 3 (1): 119–173. https://doi.org/10.1193/1.1585423.

Wang, X., and T. C. Hutchinson. 2024. "Elastic and Inelastic Acceleration Amplification of Nonstructural Components Characterized Using Recorded Building Responses." *Engineering Structures* 302:117306. https://doi.org/10.1016/j.engstruct.2023.117306.

Welch, D. P., and T. J. Sullivan. 2017. "Illustrating a New Possibility for the Estimation of Floor Spectra in Nonlinear Multi-Degree of Freedom Systems." In *16th World Conference on Earthquake Engineering*, Santiago, Chile, January, 2017, 1–12.

Xue, H., Y. Tan, and A. Sha. 2020. "Test Method on Adhesive Property of Joint Sealant in Supporting Layer of Ballastless Slab Track." *Journal of Materials in Civil Engineering* 32 (10): 4020311. https://doi.org/10.1061/(ASCE)MT.1943-5533.0003163.

Yan, Z., S. Ramhormozian, G. C. Clifton, R. Zhang, P. Xiang, L. J. Jia, G. A. MacRae, and X. Zhao. 2023. "Numerical Studies on the Seismic Response of a Three-Storey Low-Damage Steel Framed Structure Incorporating Seismic Friction Connections." *Resilient Cities and Structures* 2 (1): 91–102. https://doi.org/10.1016/J.RCNS.2023.02.007.